Journal of Solid State Chemistry 184 (2011) 3185–3189

Contents lists available at SciVerse ScienceDirect

Journal of Solid State Chemistry

journal homepage: www.elsevier.com/locate/jssc

# Structure and properties of rhombohedral $CePd_3Ga_8$: A variant of the cubic parent compound with $BaHg_{11}$ structure type

Robin T. Macaluso [a,b,*], Melanie Francisco [c], David P. Young [d], Shane Stadler [d], John F. Mitchell [b], Urs Geiser [b], Han-yul Hong [a], Mercouri G. Kanatzidis [b,c]

[a] Department of Chemistry and Biochemistry, University of Northern Colorado, Greeley, CO 80639, USA
[b] Materials Science Division, Argonne National Laboratory, 9700S. Cass Ave., Argonne, IL 60439, USA
[c] Department of Chemistry, Northwestern University, Evanston, IL60208, USA
[d] Department of Physics and Astronomy, Louisiana State University, Baton Rouge, LA 70803, USA

ARTICLE INFO

*Article history:*
Received 26 July 2011
Received in revised form
30 September 2011
Accepted 2 October 2011
Available online 8 October 2011

*Keywords:*
$BaHg_{11}$ type
Flux growth
Single-crystal X-ray diffraction
Intermetallic
$CePd_3Ga_8$

ABSTRACT

Single crystals of a new intermetallic gallide, *R*-$CePd_3Ga_8$, have been synthesized from excess molten gallium. Single-crystal X-ray diffraction reveals that *R*-$CePd_3Ga_8$ crystallizes in the *R*-3*m* space group with $a=b=c=8.4903(10)$ Å and $\alpha=\beta=\gamma=89.993(17)$. *R*-$CePd_3Ga_8$ is a variant of the cubic $BaHg_{11}$ structure type with three structural units: a Ce-centered polyhedron, a distorted cube of $Pd_2Ga_6$ and a Pd-centered cuboctahedron. The distortions of these units are compared to undistorted analogous units in intermetallic compounds with $BaHg_{11}$ structure type. Field and temperature-dependent magnetization measurements on *R*-$CePd_3Ga_8$ reveal a paramagnetic material with strong antiferromagnetic correlations and a magnetization consistent with $Ce^{3+}$. Electrical resistance measurements indicate Kondo behavior between localized $Ce^{3+}$ magnetic moments.



## 1. Introduction

The class of polar intermetallics lies between the well-known Hume-Rothery and Zintl phases [1–3] and for this reason presents a change in understanding their structures and bonding. Hume-Rothery phases are composed of Group 11 metals combined with Group 12–15 elements, and their crystal structures can be rationalized by valence electron count [4]. Zintl phases, on the other hand, have significantly large electronegativity differences and their structural features can be understood with the octet rule. As in Zintl phases, polar intermetallics also possess large electronegativity differences between constituent metals. However, their structural features cannot be easily rationalized.

In Group 13 intermetallics, aluminides are generally considered to be at the so-called Zintl phase boundary, whereas gallides are often not considered to be Zintl phases [3]. Since Al and Ga are isoelectronic, it would be reasonable to expect that intermetallic aluminides and gallides would form similar structures; however, there are actually very few examples of isostructural Al and Ga compounds. This implies that there is a significant contrast between aluminides versus gallides, and that the continued investigation of intermetallic gallium compounds is warranted. Synthesis and characterization of novel gallides may also facilitate a better understanding of the wide spectrum of bonding in intermetallics with Hume-Rothery phases characterizing one extreme and Zintl phases characterizing the other.

Polar intermetallics are often characterized by complex structures. A rich and diverse range of Ga-clusters can be formed in alkali metal-gallides, including dumbbells, icosahedra, and Samson polyhedra [1]. However, gallide clusters are generally considered complex and their chemistry still remains a challenge to the scientific community. Gallium intermetallics exhibit a wide range of interesting structure, physical properties and potential applications, ranging from heavy-fermion magnetic to semihydrogenation catalysts [5–9].

In our investigations, we have identified rhombohedral *R*-$CePd_3Ga_8$ and cubic *C*-$CePd_3Ga_8$ variants of the $BaHg_{11}$ structure type. In this paper, we report for the first time the synthesis and structure of single crystals of the *R*-$CePd_3Ga_8$. Several aluminides bearing the $BaHg_{11}$or closely related structure include $CeAg_3Al_8$ [10], $EuAg_xAl_{11-x}$ [11], $RAu_{6+x}Al_{26}T$ (R=Ca, Sr, Eu, Yb; T=early transition metal) [12], and $M_3Au_{6+x}Al_{26}Ti$ (M=Ca, Sr, Yb) [13]. $CePd_3Ga_8$ will provide opportunities to investigate the similarities and differences in aluminide versus gallide chemistry.

* Corresponding author at: Department of Chemistry and Biochemistry, University of Northern Colorado, Ross Hall, Campus Box 98, Greeley, CO 80639, USA.
*E-mail address:* robin.macaluso@unco.edu (R.T. Macaluso).

0022-4596/$ - see front matter © 2011 Elsevier Inc. All rights reserved.
doi:10.1016/j.jssc.2011.10.001

## 2. Materials and methods

### 2.1. Synthesis

Cerium (Alfa Aesar, 99.9%), palladium (Alfa Aesar, 99.95%), and gallium (Alfa Aesar, 99.999%) were used to synthesize single crystals of $CePd_3Ga_8$. Cerium powder was obtained from filing a Ce ingot in a $N_2$-filled glove box, where the powder from the surface was discarded, and only Ce powder from the interior of the ingot was used in the synthesis reactions. Palladium and gallium were used as received.

Ce filings, Pd, and Ga were added to an alumina crucible in a 1:2:20 molar ratio. The crucible and its contents were sealed in a fused silica ampoule, and then heated to 1150 °C at 65°/h in a box furnace. The ampoule dwelled at 1150 °C for 2 h before being cooled to 350 °C at a rate of 60 °C/h. The ampoule was removed from the furnace at 350 °C, and immediately inverted and placed into a centrifuge. Cooling and removing the ampoule at 300 °C yielded similar results.

Alternatively, single crystals were obtained by heating to 1000 °C, dwelling for 5 h, slow-cooling to 860 °C at 5.83 °C/h, dwelling for 60 h, and fast-cooling to 300 °C at 75 °C/h. At 300 °C, the tube was quickly inverted and centrifuged at 2800 rpm to remove excess flux. The major phase was $CePd_3Ga_8$, which was approximately 80–90% of the final product, with 10–20% of the final product as minority phases, $CePdGa_6$ and $Ce_2PdGa_{12}$. Yields were determined by relative intensities in powder X-ray diffraction patterns.

The excess liquid Ga was removed by centrifugation of the inverted ampoule for 3–5 min. An image of a typical crystal obtained by scanning electron microscopy is shown in Fig. 1. Single crystals in the alumina crucible were mechanically extracted for structural analysis and property measurements. Crystal dimensions ranged between 0.50 to 0.75 mm, with flat surfaces corresponding to the 1-1-1 face. Residual Ga flux remaining on the crystal surface was removed by placing the crystals in a 3M solution of $I_2$ in DMF. Crystals appeared to be stable in air for at least several months.

### 2.2. Diffraction

The crystal structure of $CePd_3Ga_8$ was determined using single-crystal X-ray diffraction. A $0.01 \times 0.01 \times 0.01$ mm$^3$ fragment was placed on a glass fiber with epoxy and centered in an X-ray beam with a Bruker SMART CCD diffractometer equipped with Mo $K_\alpha$ radiation ($\lambda = 0.71073$ Å) and area detector. Experimental parameters are included in Table 1. Data processing of the full data sets were performed using the program SAINT. Absorption corrections were made using SADABS [14], and crystal symmetry analysis was performed with XPREP [15]. The structure solution was obtained by direct methods and then refined by full-matrix-least-squares with the SHELXTL suite of programs [15]. Anisotropic atomic displacement parameters were refined for each site.

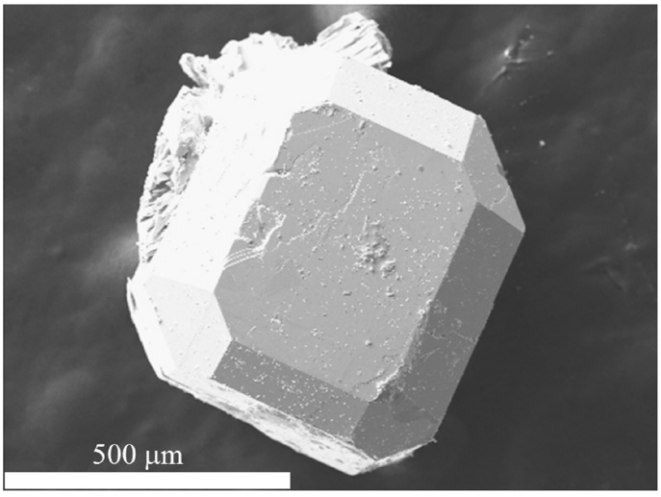


**Fig. 1.** An image of a typical flux-grown crystal of *R*-$CePd_3Ga_8$ obtained by SEM methods. The scale bar shown at the bottom of the image represents 500 μm.

**Table 1**
Structural refinement data for *R*-$CePd_3Ga_8$.

| | |
|---|---|
| Formula | $CePd_3Ga_8$ |
| Formula mass (amu) | 1017.8 |
| Space group | *R*-3*m* |
| $a=b=c$(Å) | 8.4903(10) |
| $\alpha=\beta=\gamma$ | 89.993(17) |
| $V$ (Å$^3$) | 612.02(12) |
| $Z$ | 3 |
| $T$ (K) | 293(2) |
| $\rho$ (calculated) | 8.282 |
| Crystal dimensions (mm) | $0.01 \times 0.01 \times 0.01$ |
| Radiation | Graphite monochromated MoKα |
| $\mu$ (mm$^{-1}$) | 37.735 |
| $2\theta_{\text{maximum}}$ (°) | 56.52 |
| Collected reflections | 1920 |
| Unique reflections, with $F_o^2 > 2\sigma(F_o^2)$ | 561 |
| $h$ | $-11 \le h \le 11$ |
| $k$ | $-8 \le k \le 5$ |
| $l$ | $-11 \le l \le 5$ |
| No. of variables | 39 |
| $R(F)$ for $F_o^2$ | 0.0330 |
| $R_w(F_o^2)$ | 0.0742 |
| Extinction coefficient | 0.010475 |
| $(\Delta_\rho)_{\max}$, $(\Delta_\rho)_{\min}$ (e Å$^{-3}$) | 1.833, −2.975 |

### 2.3. Elemental analysis

Elemental analysis was performed using a JEOL JSM-6610LV scanning electron microscope with energy-dispersive X-ray spectroscopy (EDX) capabilities. Crystals were mounted on an aluminum stub covered with carbon tape. Semi-quantitative analyses were performed on crystals using 20 kV accelerating voltage and an accumulation time of 180 s. Analyses of multiple spots on several crystals reveal an average composition of *R*-$Ce_{1.10(2)}Pd_{3.5(2)}Ga_{7.4(2)}$.

### 2.4. Electrical resistivity

The temperature dependence of the electrical resistance of a single crystal of $CePd_3Ga_8$ was measured using a standard 4-probe AC technique in a Quantum Design Physical Properties Measurement System (PPMS). Two-mil diameter Pt wires were attached to the sample with a 2-component conductive silver epoxy (Epotek H20E). Typical excitation currents were ~0.5 mA at a frequency of 27 Hz.

### 2.5. Magnetic susceptibility

The temperature-dependent magnetic susceptibility and field-dependent magnetization data were measured with a Quantum Design MPMS XL SQUID magnetometer. A single crystal was mounted in a plastic drinking straw and field-cooled (FC) in an applied field of 1000 Oe. The magnetization was then measured at 3 K in fields from 0 to 5 T.

## 3. Results

### 3.1. Structure determination

The experimental lattice parameters of $a=8.4672(3)$ Å and $\alpha=\beta=\gamma\sim90^\circ$ were similar to those of $YbPd_3Ga_8$, which has been reported to adopt the $BaHg_{11}$-type structure with the *Pm*-3*m* space group and $a\sim8.43$ Å [16]. However, our initial refinements with the *Pm*-3*m* space group led to very poor fits with $R1=0.3102$ for 164 reflections with $F_o>4F_o$ and $R1=0.3272$ for all the data.

Despite the similarity in lattice parameters between the title compound and $BaHg_{11}$, this poor fit has not been observed for other compounds with the cubic $BaHg_{11}$-type structure. Grin et al. attempted a model with the *Pm*-3 space group to check for additional ordering between Pd and Ga in $YbPd_xGa_{11-x}$, but instead found better statistical fits with a *Pm*-3*m* model that included mixed Pd/Ga site occupancies [16]. Our refinements of *R*-$CePd_3Ga_8$ the model with *Pm*-3 were improved from refinements with the *Pm*-3*m* model, but still provided a poor fit of $R1=0.2317$. Therefore, lower-symmetry space groups were investigated.

Additional merging of symmetry-related reflections revealed that the primitive setting of a rhombohedral lattice agreed best with the absorption-corrected reflection list. Upon checking for higher symmetry, the lowest $R_{sym}=0.0406$ corresponded to a primitive rhombohedral lattice. Least-squares refinements using *R*-3*m* provided the best fit with $R1=0.0330$ for 462 reflections with $F_o>4F_o$. The difference map was also significantly improved; the highest difference peak and hole were 1.833 and $-2.975$ $e^-/Å^3$, respectively. Further experimental details are provided in Table 1, and further details of the crystal structure investigation(s) may be obtained from Fachinformationszentrum Karlsruhe, 76344 Eggenstein-Leopoldshafen, Germany (fax: (+49)7247–808-666; e-mail: crysdata(at)fiz-karlsruhe.de, http://www.fizkarlsruhe.de/request_for_deposited_data.html) on quoting the appropriate CSD number 423347.

**Table 2**
Atomic coordinates and isotropic displacement parameters of *R*-$CePd_3Ga_8$.

| Atom | Wyckoff site | *x* | *y* | *z* | $U_{eq}$ (Å$^2$)[a] |
|---|---|---|---|---|---|
| Ce | 3*d* | 0 | 0 | 1/2 | 0.00724(31) |
| Pd1 | 6*f* | 0 | 0.33669(8) | 0.66331(8) | 0.0074(30) |
| Pd2 | 2*c* | 0.16400(11) | 0.16400(11) | 0.16400(11) | 0.00868(40) |
| Pd3 | 1*b* | 1/2 | 1/2 | 1/2 | 0.01477(58) |
| Ga1 | 6*h* | 0.35851(12) | 0.01075(17) | 0.35851(12) | 0.00881(36) |
| Ga2 | 6*g* | 0.73793(11) | 0.26207(11) | 1/2 | 0.00964(36) |
| Ga3 | 6*h* | 0.16102(12) | 0.16102(12) | 0.85757(17) | 0.00964(36) |
| Ga4 | 6*h* | 0.26832(12) | 0.26832(12) | 0.51453(17) | 0.01069(37) |

[a] $U_{eq}$ is defined as one-third of the trace of the orthogonalized $U_{ij}$ tensor.

Multiple X-ray diffraction experiments performed on various crystals from at least two different syntheses reveal the rhombohedral lattice, suggesting that the existence of crystallographic variants of *R*-$CePd_3Ga_8$ would require a different synthesis route. The kinetics and thermodynamics of other variants, including cubic-$CePd_3Ga_8$, will be discussed in a separate publication.

### 3.2. Crystal structure

*R*-$CePd_3Ga_8$ crystallizes in the space group *R*-3*m* (No. 166). In the rhombohedral setting, lattice parameters are $a=b=c=8.4903(10)$ Å and $\alpha=\beta=\gamma=89.993(17)^\circ$. Additional crystallographic details are listed in Table 2.

The structural units of *R*-$CePd_3Ga_8$ and their connectivity, shown in Figs. 2 and 3, are similar to those previously described for the $BaHg_{11}$ structure. Selected interatomic distances and bonds angles are provided in Table 3. Like $BaHg_{11}$, the structure of $CePd_3Ga_8$ can be built with three main units: Ce-centered $Pd_6Ga_{12}$ polyhedra, empty $Pd_2Ga_6$ distorted cubes and Pd-centered $Ga_{12}$ cuboctahedra. The Ce atoms form a kagomé net perpendicular to the [1 1 1] direction with Ce–Ce contacts of $\sim6.0032$ Å, which are too large to be considered as bonds.

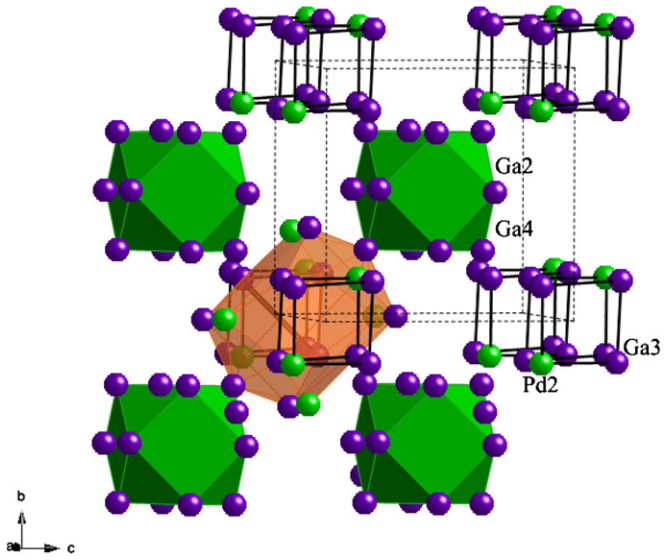


**Fig. 3.** The Ce-centered polyhedron (orange shading) shares two Ga3 corners, each with one cuboctahedra. Two distorted cubes each share a quadrilateral face with opposing sides of the Ce-polyhedron along the *c*-axis. (For interpretation of the references to colour in this figure legend, the reader is referred to the web version of this article.)

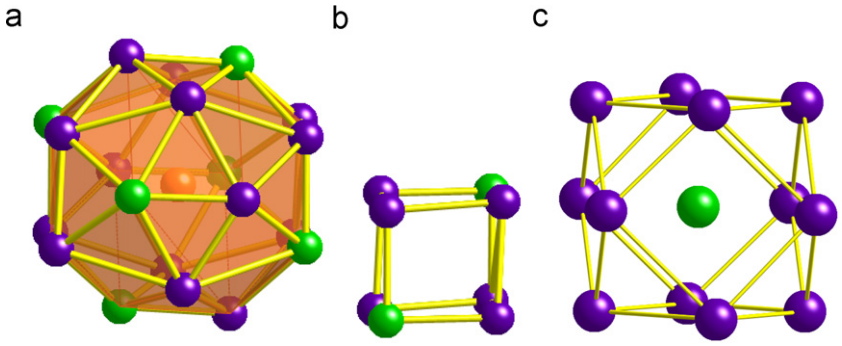


**Fig. 2.** The three structural units of *R*-$CePd_3Ga_8$ include (a) Ce-centered polyhedron, (b) distorted cube, and (c) Pd-centered cuboctahedron. Orange, green and purple spheres represent Ce, Pd, and Ga, respectively. (For interpretation of the references to colour in this figure legend, the reader is referred to the web version of this article.)

**Table 3**
Selected interatomic distances and bond angles in *R*-$CePd_3Ga_8$.

| | Distance (Å) | | Angle (deg.) |
|---|---|---|---|
| *Ce polyhedron* | | | |
| 3 * Ce–Pd1 | 3.1772(6) | Pd2–Ce–Pd2 | 180 |
| 3 * Ce–Pd2 | 3.4662(6) | Pd1–Ce–Pd1 | 79.01(3) |
| 2 * Ce–Ga1 | 3.2735(8) | Ga2–Ce–Ga2 | 180 |
| 2 * Ce–Ga2 | 3.1465(15) | Ga4–Ce–Ga4 | 180 |
| 4 * Ce–Ga3 | 3.4070(15) | Ga3–Ce–Ga3 | 47.43(3) |
| 2 * Ce–Ga4 | 3.2243(16) | | |
| *Distorted cube* | | | |
| 4 * Ga3–Ga3 | 2.7437(22) | Pd2–Ga3–Ga3 | 93.95(4) |
| 4 * Ga3–Pd2 | 2.5993(17) | | |
| *Pd cuboctahedron* | | | |
| 6 * Pd3–Ga2 | 2.8567(15) | Ga4–Pd3–Ga2 | 122.06(3) |
| 6 * Pd3–Ga4 | 2.7847(16) | | |

The Ce atoms are coordinated to 6 Pd and 12 Ga atoms, which together form an 18-vertex $Pd_6Ga_{12}$ cage surrounding the Ce atom. The Pd and Ga atoms form 32 irregular triangular faces and two quadrilaterals. Ce–Ga interatomic distances range from 3.1465(15) Å to 3.4070(8) Å. Although these distances are larger than the bond distance expected by summation of Ce and Ga covalent radii (1.65 and 1.26 Å, respectively) [17], this range is typical of Ce–Ga distances in intermetallic compounds such as $Ce_3Ga_9Ge$ [8], $Ce_2MGa_9Ge_2$ (M=Ni, Co) [9], $CePdGa_6$ [18], $Ce_2PdGa_{12}$ [6], and $Ce_2PdGa_{10}$ [7] where the Ce–Ga interatomic distances range between ~3.10 and 3.43 Å. The Ce–Pd1 interatomic distance in *R*-$CePd_3Ga_8$ measures 3.1773(6) Å, which is close to the sum of the covalent radii of Ce (1.65 Å) and Pd (1.39 Å)[17] while the Ce–Pd2 interatomic distance measures 3.4662(6) Å.

Each quadrilateral is composed of one Pd2 and three Ga3 atoms with 2 × Pd–Ga distances of 2.5994(17) Å and 2 × Ga–Ga distances of 2.744(2) Å. Opposing Pd2-Ga3-Pd2 bond angles measure 93.948, while the Ga3–Pd2–Ga3 and Ga3–Ga3–Ga3 angles measure ~88.9° and 83.1°, respectively. The two quadrilaterals of the Ce-polyhedron are shared faces with the distorted cube, which are formed by two Pd2 and six Pd3 atoms at the corners. Bond angles ranging between ~83.1° and 94.0° indicate a strongly distorted cube. This cube can be occupied by a transition metal, forming a stuffed variant of the $BaHg_{11}$ structure type [12,13].

Pd3 atoms form a cuboctahedron with six Ga2 and six Ga4 atoms. Each Ga4 serves as a shared corner between a cuboctahedron and a Ce-polyhedron. The Pd-centered cuboctahedron is also distorted with 6 × Pd3–Ga2 contacts of ~2.8567 Å and 6 × Pd3–Ga4 contacts of ~2.785 Å.

According to the International Tables of Crystallography, *R*-3*m* is a *translationengleiche* (*t*) subgroup of *Pm*-3*m* [19]. In cubic $YbPd_xGa_{11-x}$, the Pd and Ga atoms are unevenly distributed among the 12*j* and 8*g* positions (with *Pm*-3*m* space group) that form an undistorted $Pd_8$ cube [16]. In *R*-$CePd_3Ga_8$, however, the analogous unit to the $Pd_8$ cube is the $Pd_2Ga_6$ cube where Pd2 and Ga3 atoms order into sites that are crystallographically inequivalent, resulting in a distorted $Pd_2Ga_6$ cube (Fig. 2b) and loss of the three-fold rotation of the cubic unit.

$YbPd_3Ga_8$ consists of one Ga site (12*i* in *Pm*-3*m*), which is split into four atomic sites in *R*-$CePd_3Ga_8$. The Pd-centered cuboctahedron in *R*-$CePd_3Ga_8$ (Fig. 2c) is composed of two unique Ga positions (Ga2 and Ga4), whereas all the Ga in the analogous cuboctahedron in $YbPd_3Ga_8$ are identical. This difference can be observed in the range of Pd–Ga bond lengths in *R*-$CePd_3Ga_8$ and ultimately loss of rotation axes and mirror planes compared to the undistorted Pd-centered cuboctahedron in $YbPd_3Ga_8$, which can be described with one Pd–Ga bond length of ~2.803 Å.

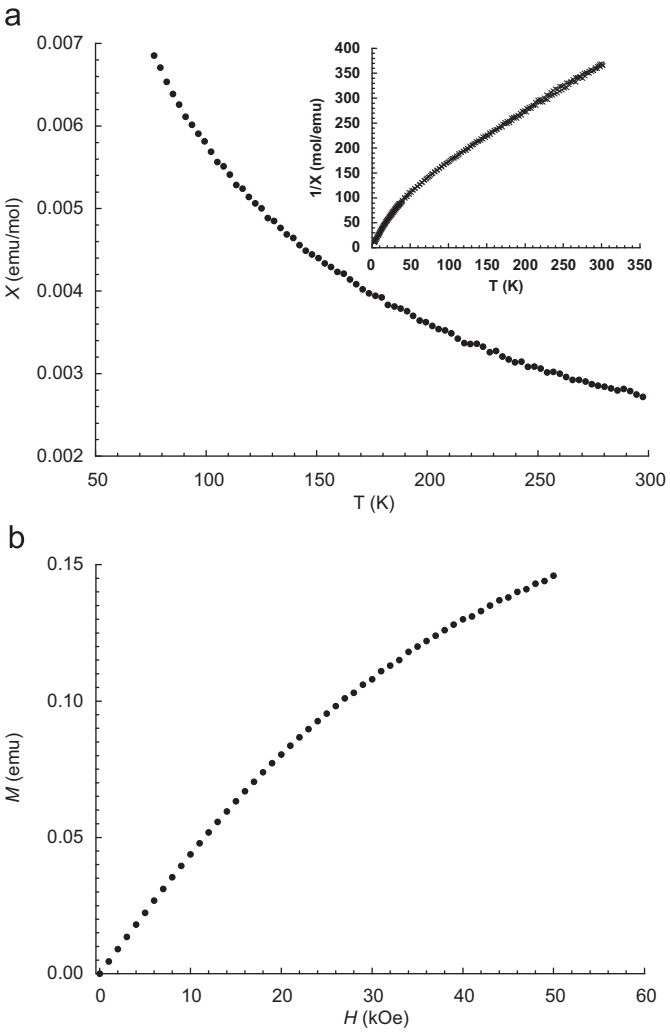


**Fig. 4.** (a) Magnetic susceptibility versus temperature of a single crystal of *R*-$CePd_3Ga_8$. (Inset shows the inverse susceptibility versus temperature. The solid line is a fit to the data as indicated in the text.) (b) Magnetization of *R*-$CePd_3Ga_8$ as a function of applied field at 3 K.

### 3.3. Magnetization

Temperature-dependent magnetization data are presented in Fig. 4a, and field-dependent magnetization data are presented in Fig. 4b. A modified Curie–Weiss law, $\chi=(C/T-\theta)+\chi_o$ (where $C$ is the Curie constant, $\theta$ is the Weiss constant, and $\chi_o$ is the temperature-independent contribution to the susceptibility) was applied to the data. Between ~65 K and 300 K, the data are well fit by the above expression, indicating that *R*-$CePd_3Ga_8$ is paramagnetic with strong antiferromagnetic correlations, where $\theta$ and $\chi_o$ were determined to be $-$ 68 K and $-1.619\times10^{-4}$ emu/mol, respectively. An effective moment of 2.38 $\mu_B$ per formula unit was calculated from the Curie constant and is slightly less than the expected moment of 2.54 $\mu_B$ per $Ce^{3+}$ ion, but within acceptable range of experimentally observed moments for $Ce^{3+}$ ions. The deviation from linearity in the inverse susceptibility below 65 K (shown in Fig. 4a inset) is usually attributed to an intermediate valence state and/or significant crystal electric fields in Ce intermetallics. A valence state existing between $Ce^{3+}$ and $Ce^{4+}$ would result in an effective moment with a value less than 2.54 $\mu_B$ per Ce ion. However, considering there is only one unique Ce site in the crystal structure, an intermediate valence state is not likely.

The valence electron count (vec) of $CePd_3Ga_8$ can then be calculated in a similar fashion to other compounds with $BaCd_{11}$ and

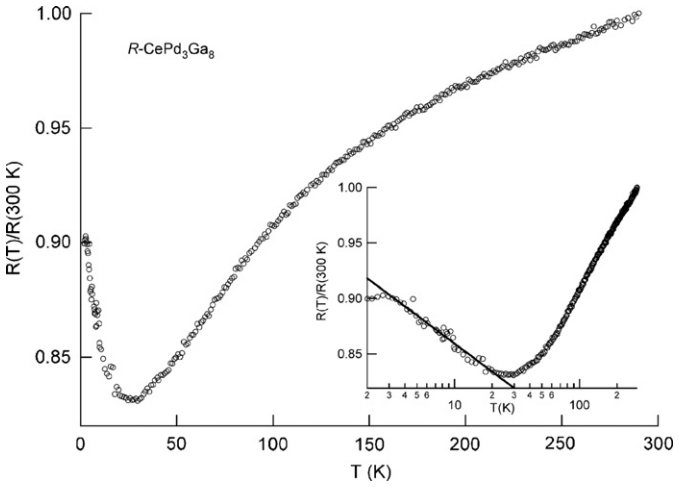


**Fig. 5.** Electrical resistance of a single crystal of *R*-$CePd_3Ga_8$ normalized to *R* (300 K). The inset shows the resistance plotted versus temperature on a log scale. The solid line is a fit to the low-temperature data as discussed in the text.

other $BaHg_{11}$ structure types as: vec=[(1 × 3)+(3 × 0)+(8 × 3)]/11=2.45 e-/atom. This vec follows the previously established general rule, where the $BaHg_{11}$ structure type is stabilized at vec values between 2.10 and 2.30 e-/atom [11]. (Pd 4*d* electrons are typically not regarded as valence electrons in the vec calculation.)

### 3.4. Electrical resistance

The normalized electrical resistance versus temperature of a single crystal of *R*-$CePd_3Ga_8$ is shown in Fig. 5. Below 300 K, the sample is metallic and displays a broad downturn in resistance below ~150 K. This type of behavior is typical in Kondo systems, where the conduction electrons interact with the local (*f*) magnetic moments. At ~30 K the resistance goes through a minimum and then sharply increases at lower temperature. The origin of this increased scattering is apparent from the inset of Fig. 5. Here the resistance is plotted versus temperature on a logarithmic scale and, although the data is somewhat noisy below 30 K, it is well fit by the solid line, where $R(T) \sim -\ln T$. This behavior is indicative of the Kondo effect, where at low temperatures the conduction electrons is strongly coupled to and scatter from the localized magnetic moments of the Ce atoms.

## 4. Conclusions

Single crystals of a new gallide intermetallic compound, *R*-$CePd_3Ga_8$, have been synthesized and characterized for the first time. This compound displays paramagnetic behavior with antiferromagnetic correlations, and transport properties similar to other strongly correlated Kondo systems.

To our knowledge, *R*-$CePd_3Ga_8$ is the first reported rhombohedral variant of the cubic $BaHg_{11}$-type, which is quite surprising since the $BaHg_{11}$ structure has been observed for $YbPd_xGa_{11-x}$. In our investigations of *R*-$CePd_3Ga_8$, we have discovered that $CePd_3Ga_8$ can crystallize in various symmetries, including cubic. We are currently exploring the synthesis (cubic) *C*-$CePd_3Ga_8$ and structure-property relationships to compare with *R*-$CePd_3Ga_8$.

## Acknowledgment

This work is supported by NSF CAREER Award 1056515 and Research Corporation Cottrell College Science Award. DPY acknowledges support of the NSF under Grant No. DMR-1005764, and SS acknowledges support of the NSF under Grant No. NSF-DMR-0545728. Financial support from the Department of Energy (DE-FG02-07ER46356) for MGK is gratefully acknowledged. Work at Argonne National Laboratory was supported by the U.S. Department of Energy, Office of Science, Basic Energy Sciences, under contract DE-AC02—06CH11357. We thank Ken Cochran and Chad Wangeline (UNC) for help with SEM.

## Appendix A. Supporting materials

Supplementary data associated with this article can be found in the online version at doi:10.1016/j.jssc.2011.10.001.

## References

[1] C. Belin, M. Tillard-Charbonnel, Prog. Solid State Chem. 22 (1993) 59.
[2] C. Belin, M. Tillard-Charbonnel, Coord. Chem. Rev. 178–180 (1998) 429.
[3] J.D. Corbett, Angew. Chem. Int. Ed. 39 (2000) 670.
[4] W. Hume-Rothery, G.V. Raynor, The Structure of Metals and Alloys, 4th ed., The Institute of Metals, London, 1962.
[5] (a) M. Armbruester, K. Kovnir, M. Behrens, D. Teschner, Y. Grin, R. Schloegl, J. Am. Chem. Soc. 132 (2010) 14745;
(b) S. Bobev, J. Hullmann, T. Harmening, R. Poettgen, Dalton Trans. 39 (2010) 6049;
(c) X.Z. Chen, P. Small, S. Sportouch, M. Zhuravleva, P. Brazis, C.R. Kannewurf, M.G. Kanatzidis, Chem. Mater. 12 (2000) 2520;
(d) R. Gumeniuk, Y. Prots, W. Schnelle, U. Burkhardt, Y. Kuz'ma, Y. Grin, J. Alloys Compds. 469 (2009) 28;
(e) R. Kraft, M. Valldor, R. Pottgen, Z. Naturforsch, B. Chem, Sci 58 (2003) 827;
(f) D. Kussmann, R.D. Hoffmann, R. Pottgen, Z. Anorg. Allg. Chemie 627 (2001) 2053;
(g) R.T. Macaluso, S. Nakatsuji, H. Lee, Z. Fisk, M. Moldovan, D.P. Young, J.Y. Chan, J. Solid State Chem. 174 (2003) 296;
(h) M.C. Menard, Y.M. Xiong, A.B. Karki, B.L. Drake, P.W. Adams, F.R. Fronczek, D.P. Young, J.Y. Chan, J. Solid State Chem. 183 (2010) 1935;
(i) A.M. Mills, A. Mar, Inorg. Chem. 39 (2000) 4599;
(j) A.M. Mills, A. Mar, J. Am. Chem. Soc. 123 (2001) 1151;
(k) M.G. Morgan, M.T. Wang, W.Y. Chan, A. Mar, Inorg. Chem. 42 (2003) 1549;
(l) S.-M. Park, S.-J. Kim, M.G. Kanatzidis, J. Solid State Chem. 177 (2004) 2867;
(m) O. Sichevych, W. Schnelle, Y. Prots, U. Burkhardt, Y. Grin, Z. Naturforsch., B: Chem. Sci. 61 (2006) 904;
(n) M.A. Zhuravleva, X.Z. Chen, X. Wang, A.J. Schultz, J. Ireland, C.K. Kannewurf, M.G. Kanatzidis, Chem. Mater. 14 (2002) 3066;
(o) M.A. Zhuravleva, M. Evain, V. Petricek, M.G. Kanatzidis, J. Am. Chem. Soc. 129 (2007) 3082;
(p) M.A. Zhuravleva, R.J. Pcionek, X. Wang, A.J. Schultz, M.G. Kanatzidis, Inorg. Chem. 42 (2003) 6412;
(q) M.A. Zhuravleva, R.J. Pcionek, X. Wang, A.J. Schultz, M.G. Kanatzidis, Inorg Chem 42 (2003) 6412;
(r) M.A. Zhuravleva, X. Wang, A.J. Schultz, T. Bakas, M.G. Kanatzidis, Inorg. Chem. 41 (2002) 6056.
[6] R.T. Macaluso, J.N. Millican, S. Nakatsuji, H.O. Lee, B. Carter, N.O. Moreno, Z. Fisk, J.Y. Chan, J. Solid State Chem. 178 (2005) 3547.
[7] J.N. Millican, R.T. Macaluso, D.P. Young, M. Moldovan, J.Y. Chan, J. Solid State Chem. 177 (2004).
[8] M.A. Zhuravleva, M.G. Kanatzidis, J. Solid State Chem. 173 (2003) 280.
[9] M.A. Zhuravleva, M.G. Kanatzidis, Inorg. Chem. 47 (2008) 9471.
[10] G. Cordier, G. Dörsam, R. Kniep, J. Magn. Magn. Mater. 76 & 77 (1988) 653.
[11] F. Wang, K.N. Pearson, W.E. Straszheim, G.J. Miller, Chem. Mater. 22 (2010) 1798.
[12] S.E. Latturner, B. Daniel, S.D. Mahanti, M.G. Kanatzidis, Inorg. Chem. 48 (2009) 1346.
[13] S.E. Latturner, M.G. Kanatzidis, Inorg. Chem. 43 (2004) 2.
[14] SAINT, version 6.02; Bruker AXS, Inc.: Madison, WI, 2000.
[15] G.M. Sheldrick, Acta Cryst. A 64 (2008) 112.
[16] Y.N. Grin, K. Hiebl, P. Rogl, C. Godart, E. Alleno, J. Alloys Compds. 252 (1997) 88.
[17] J.C. Slater, J. Chem. Phys. 39 (1964) 3199.
[18] R.T. Macaluso, S. Nakatsuji, H. Lee, Z. Fisk, M. Moldovan, D.P. Young, J.Y. Chan, J. Solid State Chem. 174 (2003) 296.
[19] T. Hahn, International Tables of Crystallography, vol. A., International Union of Crystallography, 2005.